High performance broadband photodetectors based on Sb_2Te_3/n-Si heterostructure

Yuping Zhang[1,2], Libin Tang[1,2,a)] and Kar Seng Teng [3,b)]

[1] Kunming Institute of Physics, Kunming 650223, People's Republic of China
[2] Yunnan Key Laboratory of Advanced Photoelectric Materials & Devices, No.31 East Jiaochang Road, 650223, Kunming, People's Republic of China
[3] College of Engineering, Swansea University, Bay Campus, Fabian Way, Swansea SA1 8EN, United Kingdom

E-mail: scitang@163.com (L. B. Tang), k.s.teng@swansea.ac.uk (K. S. Teng)

Abstract

With the rapid development of optoelectronic devices, photodetectors have triggered an unprecedented promising in the field of optical communication, environmental monitoring, biological imaging, chemical sensing. At the same time, there is a higher requirement for photodetectors. It is still a huge challenge for photodetectors that possess excellent performance, low cost and broad range photoresponse from ultraviolet to infrared. In this work, a facile, low cost growth of Sb_2Te_3 thin film using magnetic sputtering was performed. After rapid annealing treatment, the crystallinity of the thin film was transformed from amorphous to polycrystalline. Ultraviolet-visible-infrared absorption study of the thin film revealed broad absorption range, which is ideal for use in broadband photodetectors. Such photodetectors can find many important applications in communication, data security, environmental monitoring and defense technology etc. A prototype photodetector, consisting of Sb_2Te_3/n-Si heterostructure, was produced and characterized. The device demonstrated a significant photoelectric response at a broad spectral range of between 250 and 2400 nm. The maximum responsivity and detectivity of the device were 270 A/W and 1.28×10^{13} Jones, respectively, under 2400 nm illumination. Therefore, the results showed the potential use of Sb_2Te_3 thin film in developing high performance broadband photodetectors.

Keywords: photodetector, Sb_2Te_3, broadband

1. Introduction

Photodetectors have the ability to convert light into electrical signals, which plays an important role in various fields, such as biomedical, display, environmental monitoring, optical communications, security, industrial process control, and astronomical observation[1,2]. In recent years, the high-performance broadband photodetectors have drawn much attention in detectors. Generally, detecting different spectral bands requires different materials with suitable bandgaps. Therefore, the commonly used strategy is selecting suitable semiconductors with broadband absorption for photodetectors. Many attempts have been made for both organic and inorganic active materials, such as graphene[3], black phosphorus[4], perovskite[5,6], transition metal dichalcogenides[7], and dirac semimetal[8]. Huang et al. fabricated a graphene/Si photodetector with the high responsivity (26 A/W) and a very fast photoresponse(78 ns)[9]. In addition, Hu et al. improved the performance of

graphene/Si photodetectors by covering random platinum nanoparticles on top of the devices[10]. Due to plasma effect, the responsivity of the devices can reach up to 1.68×10^7 A/W. Meanwhile, topological insulator has attracted broad interest in recent years due to its many exciting electronic and physical properties. It is considered as a new quantum material exhibiting many novel properties, which are completely different from traditional metals and insulators[11]. In particular, its unique electronic and optical properties are ideal for the development of broad band photodetector[12-14].

Examples of topological insulators are Bi_2Se_3, Bi_2Te_3 and Sb_2Te_3 as confirmed by both theoretical and experimental studies[15,16]. To date, bismuth based compounds, such as Bi_2Se_3 and Bi_2Te_3, are the most commonly studied topological insulators that used in the development of broad band photodetectors[17-20]. Sb_2Te_3 is not a new material as there have been many studies on its thermoelectric properties. The main applications of Sb_2Te_3 are in thermoelectric devices[21], phase change memories[22] and contact electrodes[23]. Only recently, there have been some reports on the use of Sb_2Te_3 as topological insulator in the field of photodetection. For example, Zheng et al. reported a near-infrared photodetector based on Sb_2Te_3 film topological insulator[24], which exhibited good response to 980 nm light with a responsivity of 21.7 A/W, thus demonstrating the potential application of Sb_2Te_3 in the field of photodetectors. Common deposition methods used in preparing topological insulator films for photodetection application are molecular beam epitaxy (MBE), chemical vapor deposition (CVD), metal organic chemical vapor deposition (MOCVD) and laser pulse deposition etc[24-26]. However, there is limited study on the use of magnetron sputtering in the preparation of topological insulator films for photodetectors. Thin film deposition by means of magnetron sputtering offers many advantages, such as facile process, low cost, low substrate temperature and good film-substrate bonding force. Herein, the use of magnetron sputtering to prepare Sb_2Te_3 thin films for the production of photodetector was investigated.

In this letter, Sb_2Te_3 films were prepared by magnetron sputtering. The as-prepared films were rapidly annealed to improve their crystallinity. A prototype photodetector with p-n junction was produced by depositing the film on n-Si substrate. The device exhibited photoelectric response over a broad spectral range between 250 and 2400 nm. Responsivity (R) of the device reached 270 A/W under 2400 nm illumination with a power density of 1.868 $\mu W/cm^2$. The device also displayed a high detectivity of 1.28×10^{13} Jones with excellent response performances from ultraviolet to near-infrared. Therefore, the preparation of Sb_2Te_3 films using magnetron sputtering can lead to high detectivity, high sensitivity and wide spectrum photodetectors.

2. Experimental

The deposition process of Sb_2Te_3 film by magnetron sputtering is relatively simple. Firstly, n-Si substrate was pre-cleaned in an ultrasonic bath with ethanol, acetone, and deionized water for 30 min sequentially. After washing and drying, it was placed in a magnetron sputtering system. The Sb_2Te_3 target was available commercially.

3. Results and discussion

The process of magnetron sputtering is shown in Fig. 1(a). Argon ions generated from argon gas are attracted to the target at high energy. These high energy ions bombarded the target resulting in sputtering of atoms or atomic groups onto a substrate surface that can lead to formation of thin film on the substrate. Annealing the substrate during deposition can promote diffusion of atoms or radicals on the substrate to improve uniformity of the deposited film. It is worth noting that the physical properties of the film prepared by magnetron sputtering can be influenced by the sputtering power. Fig. 1(b) and (c) are AFM images of unannealed films with RMS roughness of 0.792 nm and 6.837 nm deposited using sputtering power of 120 W and 200 W, respectively. At low sputtering power, the as-prepared film exhibited small surface roughness and good uniformity. The film was characterized using X-ray diffraction (XRD) to investigate its crystallinity and phase. The unannealed film did not reveal characteristic diffraction peaks (Figure S1). It was then subjected to rapid annealing treatment at a temperature of 300 ° C for 10 min. Fig. 1(d) shows the XRD results after annealing of films deposited at different sputtering powers. The characteristic peaks appeared at 2θ of 17.41°, 26.35° , 38.29°, 44.59°, 63.19°, 71.11°and 82.03°, correlated well with (006), (009), (1010), (0015), (1019), (0216) and (1214) lattice planes of PDF#15-0874 standard cards. This is in good agreement with previously reported work[27]. There was an increase in the intensity of the diffraction peaks, which suggests an improvement in crystallinity of the film, as a result of increasing sputtering power. Interestingly, the peak intensity of (006) and (1214) lattice planes for film deposited using sputtering power of 200 W was smaller than those peaks from film deposited using sputtering power of 120 W. This indicates the growth of the lattice planes might be selective depending on the sputtering power. However, this will not be studied in-depth in this work. The effect of annealing treatment on the crystallinity of the film was further investigated using transmission electron microscopy (TEM). Fig. 1(e) and (f) are low-resolution TEM images of unannealed and rapid annealed films, respectively. Fig. 1(g) and (h) are corresponding electron diffraction patterns of the films. It was found that the as-grown unannealed film prepared by magnetron sputtering was amorphous and it became polycrystalline after rapid annealing treatment. The polycrystalline diffraction ring, shown in Fig. 1(h), also

revealed the presence of Sb diffraction ring in addition to patterns associated with Sb_2Te_3. This could possibly due to segregation of Sb or volatilization of Te. High resolution TEM images are shown in Fig. 1(i)-(l), where Fig. 1(j)-(l) show selected regions in (i). A polygonal grain can be seen in Fig. 1(i) with significant lattice fringes and grain boundaries. The spacing of lattice fringes in Fig. 1(j) was 0.215 nm, which corresponded to the (110) lattice plane of Sb_2Te_3. Fig. 1(k) and (l) are images taken at the boundary of two and three grains, respectively, which show that the film was polycrystalline after annealing.

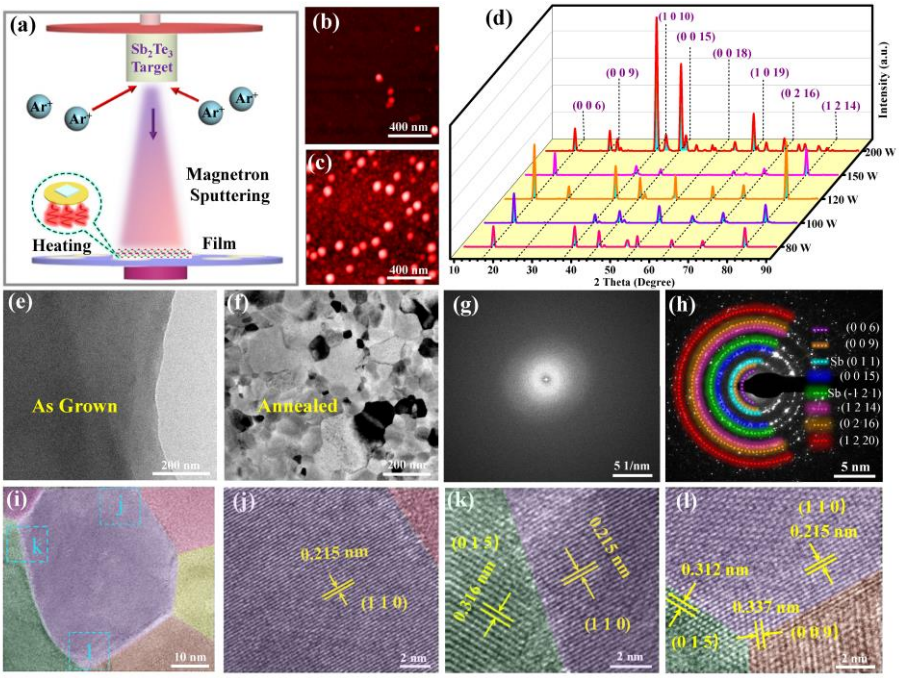

Figure 1. Schematic diagram on Sb_2Te_3 film preparation and structural characterization on the film. (a) Preparation process of Sb_2Te_3 thin film by magnetron sputtering. (b) and (c) AFM images of Sb_2Te_3 films sputtered at 120 and 200W, respectively. (d) XRD pattern of Sb_2Te_3 film sputtered at different powers. (e) Low resolution TEM image of as-grown film. (f) Low resolution TEM image of annealed film. (g) Electron diffraction pattern of the as-grown film. (h) Electron diffraction pattern of the annealed film. (i)-(l) HRTEM images of the annealed film.

It is evident that the Sb_2Te_3 film prepared by magnetron sputtering became polycrystalline by rapid annealing treatment. The microstructure of a single grain was studied from the high-resolution TEM image of the grain in Fig. 2(a). The measured lattice spacing of 0.331 nm, 0.268 nm and 0.364 nm, corresponded to the (009), (018) and (102) planes of Sb_2Te_3, respectively. Furthermore, the angles of the three crystal planes are consistent with theoretical values as shown in Supplementary Materials. Fig. 2(b) shows line profiles of circled spots in the direction of three different colored lines in Fig. 2(a). These profiles are equivalent to the hexagonal lattice of Sb_2Te_3. Fig. 2(c) shows Raman spectra of Sb_2Te_3 films under different deposition conditions. The measurements were acquired using a Renishaw in Via Raman microscope with an argon-ion laser at an excitation wavelength of 514 nm. Four Raman vibrational modes of Sb_2Te_3 are illustrated in Fig. 2(d)[28,29]. As shown in Fig. 2(c), the Sb_2Te_3 films deposited at different sputtering powers have two vibrational modes at 123 and 142 cm^{-1}, but they were not consistent with the vibration modes of Sb_2Te_3. However, a strong E_{2g} vibration mode at 113 cm^{-1} relating to Sb_2Te_3 was observed for film deposited at a sputtering power of 150 W. Furthermore, its vibration modes at 123 cm^{-1} and 142 cm^{-1} were smaller than those for film obtained at sputtering power of 200 W. Yang et al. studied the stability of two-dimensional GaTe materials[30] and found two new strong Raman peaks appeared at 126 cm^{-1} and 142 cm^{-1} after storing the GaTe film for 2 weeks. These peaks were associated with a layer of TeO_2 at the surface of the film. Increasing the sputtering power for film deposition would lead to an increase in the surface roughness of the film, which could make it easier to oxidize. Therefore, the films might have been oxidized during the preparation process. Elemental composition of the Sb_2Te_3 film deposited at sputtering power of 150 W was investigated using X-ray photoelectron spectroscopy (XPS). Fig 2(e) shows the XPS spectrum of Sb 3d core level, which consisted of $Sb3d_{3/2}$ (oxide), $Sb3d_{3/2}$ (metal), $Sb3d_{5/2}$ (oxide) and $Sb3d_{5/2}$ (metal) peaks with binding energies at 539.6 eV, 538 eV, 530.3 eV and 528.8 eV, respectively. The XPS spectrum of Te 3d core level is shown in Fig. 2(e), which consisted of $Te3d_{3/2}$ (TeO_2), $Te3d_{3/2}$ (metal), $Te3d_{5/2}$ (TeO_2) and $Te3d_{5/2}$ (metal)

peaks with binding energies at 586.8 eV, 583 eV, 576.3 eV and 572.6 eV, respectively. The XPS spectra are consistent with those reported by Georg Bend et al[31]. Although oxides were observed from XPS and Raman characterizations on the prepared Sb_2Te_3 film, they were not shown on the TEM and XRD characterizations. Therefore, this implies that the deposited films were Sb_2Te_3 and have a thin oxide layer at the surface of the film.

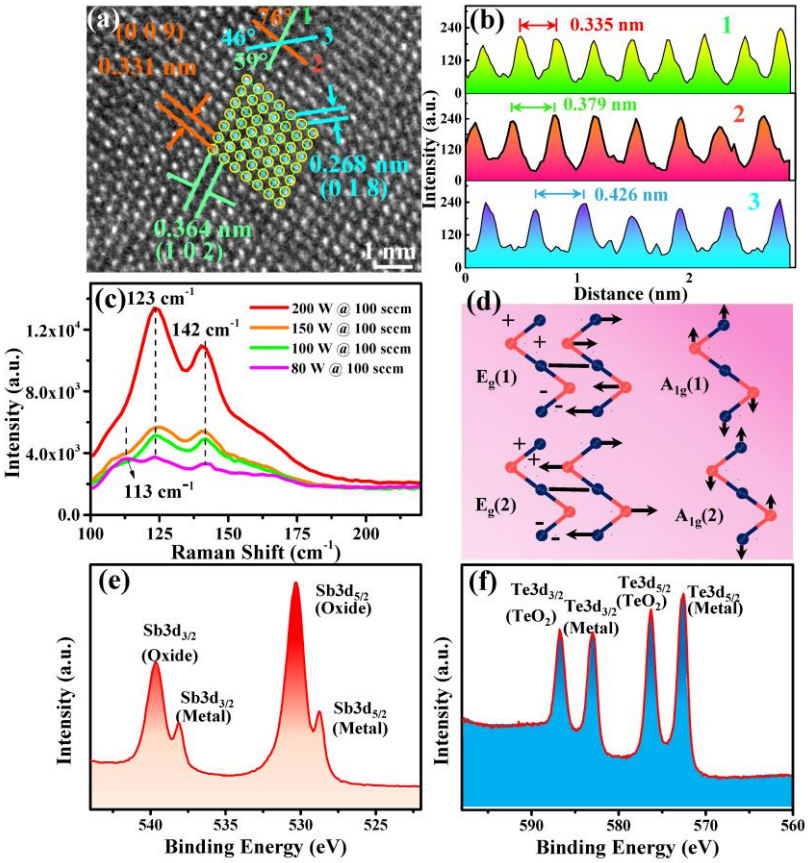

Figure 2. Phase analysis of the Sb_2Te_3 film. (a) HRTEM image showing lattice fringes of the film. (b) Line profiles corresponding to the probed positions along lines 1-3 marked in (a). (c) Raman spectroscopy of the film. (d) Schematic diagram illustrating the displacement patterns of phonons. (e)-(f) XPS spectra of Sb and Te core levels of the Sb_2Te_3 film.

In order to understand the optical properties of the Sb_2Te_3 film, ultraviolet-visible (UV-Vis) absorption spectra of the film was investigated. As shown in Fig. 3(a), the broad absorption range of the film suggests that it can be used as an absorbing layer for broadband photodetectors. The UV-Vis absorption spectra revealed that the absorption peak of the films was red-shifted when the films were annealed at higher temperature, which could due to a change in their crystallinity at higher annealing temperature. The photoelectric response characteristics of the Sb_2Te_3 film were also studied. The film was deposited on n-Si substrate by magnetron sputtering. An Al electrode was then covered over the surface of Sb_2Te_3 film and n-Si substrate. A small window, acting as photosensitive region, was created on the Al electrode above the Sb_2Te_3 film to increase the collection efficiency of charge. The structure of the photodetector is illustrated in Fig. 3(b), and the optical image of the device is inserted in Fig. 3(d). The optimized Sb_2Te_3 thin film for fabricating device was sputtering for 200 s at a sputtering power of 120 W followed by annealing at 300 °C for 10 min. The thickness of the deposited Sb_2Te_3 film was measured by AFM and used to estimate the optical band gap of the film. The film, shown in Fig. 3(c), was obtained by using a sputtering power of 120 W for 200 s and has a thickness of about 114 nm. The Sb_2Te_3 films deposited at sputtering power of 120W exhibited good crystallinity and uniformity as well as small surface roughness, which could minimize surface oxidation. Since the Sb_2Te_3 film is a direct band gap material[32], its optical band gap can be calculated using the following formula:

$$\alpha(h\nu)=B(h\nu-E_g)^{1/2} \quad (1)$$

where α is molar absorption coefficient, h is Planck constant, ν is frequency of incident photon, B is a constant, and E_g is optical band gap of the semiconductor. As shown in Fig. 3(c), optical band gap of the Sb_2Te_3 film was calculated to be 0.54 eV after linear fitting, which is larger than previously reported band gap of 0.45 eV[33]. This might be due to the relatively small thickness of the film that could

affect its optical bandgap. A plot of *I-V* characteristic curve of the device measured under dark conditions and at a wavelength of 2400 nm with power density of 1.0868 μW/cm^2 is shown in Fig. 3(d). An increase in current of the device was observed under illumination, hence exhibiting good photoelectric response and ohmic contact behavior. The *R* and *D** of the device were calculated by the following equations[34]:

$$R=J_{ph}/Popt \quad (2)$$

$$D^*=R/(2q|J_{dark}|)^{1/2} \quad (3)$$

where J_{ph} is photocurrent density, P_{opt} is incident light power density, q is unit charge, and J_{dark} is dark current density. The calculated result is shown in Fig. 3(e) revealing maximum value of *R* and *D** as 270 A/W and 1.28×10^{13} Jones (1 Jones=1 cm Hz$^{1/2}$ W^{-1}), respectively. The detection mechanism of the device is illustrated in Fig. 3(f). The Sb_2Te_3 has zero-band gap surface states and the presence of these states is essential in achieving a broadband response spectrum. The Sb_2Te_3 film is a p-type material and forms a p-n junction with the n-type silicon substrate. As a result of light absorption at the Sb_2Te_3 film, photogenerated carriers are generated and quickly separated by the built-in electric field to produce a current. The built-in electric field would also increase the lifetime of the photogenerated carriers. Fig. 3(g) shows the photoelectric response time of the device. Under 940 nm illumination, the device exhibited good sensitivity and stability. The rise and fall times of photogenerated carriers were 129.8 ms and 132.2 ms, respectively. The response rate is relatively higher than the device reported by Zheng et al[24]. In order to investigate the cyclic light response characteristics of the device under different illuminations, the transient responses at 390, 555, 660, 740, 850 and 940 nm were studied. As shown in Fig. 3(h), the device demonstrated good response and stability at different light wavelengths. The difference in device off-state current was mainly caused by different bias voltages. The response range of the device was examined from the *I-V* characteristic curve obtained under light illumination over a broad wavelength range between 250 and 2400 nm, as shown in Fig. 3(i). The plot also showed that the photocurrent generated by illumination increases with increasing power density. Table 1 compares the performances, such as response spectral range, carrier rise and fall times, responsivity and detectivity, of the device in this work with previously reported photodetectors based on Sb_2Te_3, Bi_2Se_3, Bi_2Te_3 and graphene. In this work, the spectral range of the device was broader, and the *R* and *D** were also higher than previously reported Sb_2Te_3 based photodetectors. Thus, the device in this work demonstrated an excellent photodetection performances[35,36].

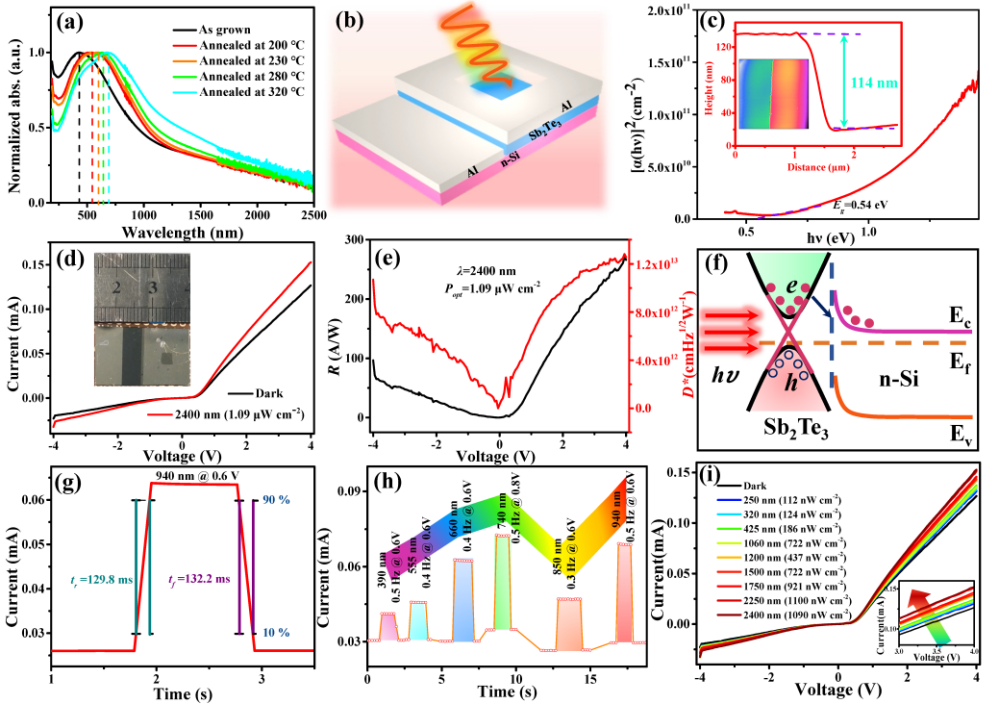

Figure 3. (a) UV-vis absorption spectra of the Sb_2Te_3 film annealed at different temperatures. (b) Schematic diagram of Sb_2Te_3/n-Si photodetector structure. (c) Plot used to obtain optical band gap of the film (Inset: AFM line profile showing thickness measurement). (d) *I-V* measurements under dark and 2400 nm light source (Inset: the optical image of the device). (e) Plot of Responsivity (*R*) and Detectivity (*D**) against V. (f) Schematic illustrating the photodetection mechanism. (g) Photocurrent switching behavior of Sb_2Te_3/n-Si at 0.5 V bias illuminated with a 940 nm light source. (h) Photocurrent switching behavior of Sb_2Te_3/n-Si illuminated with different wavelengths of light and at different biases. (i) *I-V* characteristics of the device measured under a broad wavelength range of light sources.

Table 1. Comparison on the performances of photodetectors based on Sb_2Te_3, Bi_2Te_3, Bi_2Se_3 and graphene.

Materials	Wavelength (nm)	t_r (ms)	t_f (ms)	R (A/W)	D^*(Jones)	Ref.
Sb_2Te_3 / Si	250-2400	129.8 (940nm)	132.2 (940nm)	270 (@2400nm)	1.28×10^{13}	This Work
Sb_2Te_3	980	238.7×10^{3}	203.5×10^{3}	21.7	1.22×10^{11}	[24]
Sb_2Te_3 / STO	405-1550	30×10^{-3}	95×10^{-3}	4.8×10^{-3} (@405 nm)	8.6×10^{10}	[35]
Sb_2Te_3 / Si	520-980	14.22	8.2	1.36×10^{-3}	-	[36]
Bi_2Te_3 / WS_2	370-1550	-	-	30.7	2.3×10^{11}	[37]
Bi_2Te_3 / Pentacene	450-3500	-	-	14.89	-	[20]
Graphene /Bi_2Te_3 Nanowire	940-1720	-	-	$\sim10^{6}$	$\sim10^{11}$	[19]
Bi_2Se_3 / Si-Nanowire	890	-	-	934.1	2.3×10^{13}	[38]
Bi_2Se_3 / Si	808	2.5×10^{-3}	5.5×10^{-3}	24.28	4.39×10^{12}	[39]
Graphene / Si	300-1100	4×10^{-5}	4×10^{-5}	26	-	[9]
Graphene / Si	-	1.8×10^{-4}	-	1.68×10^{7}	-	[10]

4. Conclusion

In conclusion, Sb_2Te_3 thin film was prepared by magnetron sputtering. After rapid annealing at 300 °C for 10 min, the film changed from amorphous to polycrystalline state with great improvement in its crystallinity. A prototype p-n junction photodetector based on Sb_2Te_3/n-Si heterostructure was produced and demonstrated excellent broad spectral response between 250 and 2400 nm. Under 2400 nm illumination, the maximum value of R and D^* of the device reached 270 A/W and 1.28×10^{13} Jones, respectively. Such device performances were far better that previously reported Sb_2Te_3 film-based photodetector. The transient performance of the device was also studied at different wavelengths and bias voltages, which indicates that the Sb_2Te_3 is a promising material for developing high-performance broadband photodetectors.

See Supplementary Materials for XRD characterization of unannealed film (Supplementary Figure S1), calculated angles of the three crystal planes (Supplementary Table S1), and the electrical parameters of Sb_2Te_3 films (Supplementary Table S2).

Acknowledgements

This work was supported by National Natural Science Foundation of China (Grant Nos. 61106098 and 51462037) and Yunnan Key Laboratory of Advanced Photoelectric Materials & Devices, China.

References

[1] Fang H J, Xu C, Ding J, Li Q, Sun J L, Dai J Y, Ren T L and Yan Q F 2016 self-powered ultrabroadband photodetector monolithically integrated on a PMN-PT ferroelectric single crystal *ACS Appl. Mater. Interfaces* **8** 32934

[2] Wang J, Ullbrich S, Hou J L, Spoltore D, Wang Q W, Ma Z, Tang Z and Vandewal K 2019 organic cavity photodetectors based on nanometer-thick active layers for tunable monochromatic spectral response *ACS Photonics* **6** 1393

[3] Lan C Y, Li C, Wang S A, He T Y, Zhou Z F, Wei D P,Guo H Y, Hao Yang and Liu Y 2017 high responsive and broadband photodetectors based on WS_2-graphene van der Waals epitaxial heterostructures *Journal of Materials Chemistry C* **5** 1494

[4] Huang M Q, Wang M L, Chen C, Ma Z W, Li X F, Han J B, and Wu Y Q 2016 broadband black-phosphorus photodetectors with high responsivity *Adv. Mater.* **28** 3481

[5] Tong S C, Sun J, Wang C H, Huang Y L, Zhang C J, Shen J Q, Xie H P, Niu D M, Xiao S, Yuan Y B, He J, Yang J L and Gao Y L 2017 high-Performance broadband perovskite photodetectors based on $CH_3NH_3PbI_3$/C8BTBT heterojunction *Adv. Electron. Mater* **3** 1700058

[6] Yang X G, Liu Y, Lei H X and Li B J 2016 organic-inorganic broadband photodetector based on a single polyaniline nanowire doped with quantum dots *Nanoscale* **8** 15529

[7] Li L, Wang W K, Chai Y, Li H Q, Tian M L and Zhai T Y 2017 few-layered PtS_2 phototransistor on h-BN with high gain *Adv. Funct. Mater.* **27** 1701011

[8] Wang Q S, Li C Z, Ge S F, Li J G, Lu W, Lai J W, Liu X F, Ma J C, Yu D P, Liao Z M and Sun D 2017 ultrafast broadband photodetectors based on three-dimensional dirac semimetal Cd_3As_2 *Nano Letters* **17** 834

[9] Huang K, Yan Y C, Khan A, Zhang H, Pi X D, Yu X G and Yang G R 2017 high and fast response of a graphene-Silicon photodetector coupled with 2D fractal platinum nanoparticles *Adv. Optical Mater.* **6** 1700793

[10] Hu M, Yan Y C, Huang K, Khan A, Qiu X D, Xu D K, Zhang H, Yu X G and Yang D R 2018 performance improvement of graphene/Silicon photodetectors using high work function metal nanoparticles with plasma effect *Adv. Optical Mater.* **6** 1701243

[11] Yang J, Yu W Z, Pan Z H, Yu Q, Yin Q, Guo L, Zhao Y F, Sun T, Bao Q L and Zhang K 2018 ultra-broadband flexible photodetector based on topological crystalline insulator SnTe with high respomsivity *Small* **14** 1802598

[12] He X W, Fujimura N, Lloyd J M, Erickson K J, Talin A A, Zhang Q, Gao W L, Jiang Q J, Kawano Y, Hauge R H, Léonard F and Kono J 2014 Carbon Nanotube Terahertz Detector *Nano Lett.* **14** 3953

[13] Chen Z F, Li X M, Wang J Q, Tao L, Long M Z, Liang S J, Ang L K, Shu C, Tsang H K and Xu J B 2017 synergistic effects of plasmonics and electron trapping in graphene short-wave infrared photodetectors with ultrahigh responsivity *ACS Nano* **11** 430

[14] Chen H Y, Liu H, Zhang Z M, Hu K and Fang X S 2016 nanostructured photodetectors: from ultraviolet to terahertz *Adv. Mater.* **28** 403

[15] Zhang H J, Liu C X, Qi X L, Dai X, Fang Z and Zhang S C 2009 topological insulators in Bi_2Se_3, Bi_2Te_3 and Sb_2Te_3 with a single dirac cone on the surface *Nature Physics* **5** 438

[16] Xia Y, Qian D, Hsieh D, Wray L, Pal A, Lin H, Bansil A, Grauer D, Hor Y S, Cava R J and Hasan M Z 2009 observation of a large-gap topological-insulator class with a single Dirac cone on the surface *Nature Physics* **5** 398

[17] Tang W W, Politano A, Guo C, Guo W L, Liu C L, Wang L, Chen X S and Lu W 2018 ultrasensitive room-temperature terahertz direct detection based on a Bismuth Selenide topological insulator *Adv. Funct. Mater.* **28** 1801786

[18] Wang F K, Li L G, Huang W J, Li L, Jin B, Li H Q and Zhai T Y 2018 submillimeter 2D Bi_2Se_3 flakes toward high-performance infrared photodetection at optical communication wavelength *Adv. Funct. Mater.* **28** 1802707

[19] Islam S, Mishra J K, Kumar A, Chatterjee D, Ravishankar N and Ghosha A 2019 ultra-sensitive graphene-bismuth telluride nano-wire hybrids for infrared detection *Nanoscale* **11** 1579

[20] M. Yang M, J. Wang J, Zhao Y F, He L, Ji C H, Liu X C, Zhou H X, Wu Z M, Wang X R and Jiang Y D 2019 three-dimensional topological insulator Bi_2Te_3/organic thin film heterojunction photodetector with fast and wideband response from 450 to 3500 nanometer *ACS Nano* **13** 755

[21] Jang E, Poosapati A and Madan D 2018 enhanced thermoelectric properties of F4TCNQ doped P3HT and its use as a binder for Sb_2Te_3 based printed thermoelectric films *ACS Appl. Energy Mater.* **1** 1455

[22] Li Z, Si C, Zhou J, Xu H B and Sun Z M 2016 yttrium-doped Sb_2Te_3: a promising material for phase-change memory *ACS Appl. Mater. Interfaces* **8** 26126

[23] Liang F X, Liang L, Zhao X Y, Luo L B, Liu Y H, Tong X W, Zhang Z X and Andrew Huang J C 2018 a sensitive broadband (UV-vis-NIR) perovskite photodetector using topological insulator as electrodes *Adv. Optical Mater.* **7** 1801392

[24] Zheng K, Luo L B, Zhang T F, Liu Y H, Yu Y Q, Lu R, Qiu H L, Li Z J and Andrew Huang J C 2015 optoelectronic characteristics of a near infrared light photodetector based on a topological insulator Sb_2Te_3 film *J. Mater. Chem. C.* **3** 9154

[25] Peranioa N, Winklerb M, Bessasc D, Aabdina Z, Königb J, Böttnerb H, Hermannc R P and Eibl O 2012 room-temperature MBE deposition, thermoelectric properties, and advanced structural characterization of binary Bi_2Te_3 and Sb_2Te_3 thin films *Journal of Alloys and Compounds* **521** 163

[26] Hilmi I, Lotnyk A, Gerlach J¨urgen W, Schumacher P and Rauschenbach B 2017 research update: van-der-Waals epitaxy of layered chalcogenide Sb_2Te_3 thin films grown by pulsed laser deposition *APL Mater.* **5** 050701

[27] Motter J P, Koski K J and Cui Y 2014 general strategy for zero-valent intercalation into two-dimensional layered nanomaterials *Chem. Mater.* **26** 2313

[28] Shahil K M F, Hossain M Z, Goyal V and Balandin A A 2012 micro-raman spectroscopy of mechanically exfoliated few-quintuple layers of Bi_2Te_3, Bi_2Se_3, and Sb_2Te_3 materials*Journal of applied physics* **111** 54305

[29] Sosso G C, Caravati S and Bernasconi M 2009 vibrational properties of crystalline Sb_2Te_3 from first principles *J. Phys.: Condens. Matter* **21** 095410

[30] Yang S J, Cai H, Chen B, Ko C H, Özçelik V O, Ogletree D F, White C E, Shen Y X and Tongay S 2017 environmental stability of 2D anisotropic tellurium containing nanomaterials: anisotropic to isotropic transition *Nanoscale* **9** 12288

[31] Schaumann J, Loor M, Ünal D, Mudring A, Heimann S, Hagemann U, Schulz S, Maculewicz F and Schierning G 2017 inproving the ZT value of themoelectrics by nanostructuring: tuning the nanoparricle morphology of Sb_2Te_3 by ionic liquids *Dalton Transactions* **46** 656

[32] Zhang S L, Zhou W H, Ma Y D, Ji J P, Cai B, Yang S Y A, Z. Zhu, Chen Z F and Zeng H B 2017 tntimonene oxides: emerging tunable direct bandgap semiconductor and novel topological insulator *Nano Lett.* **17** 3434

[33] Kumar S, Singh D, Sandhu S and Thangaraj R 2012 structural, electrical, and optical properties of thermally evaporated Ge-Te, Ge-Sb-Te, and Sb-Te thin films *Phys. Status Solidi A* **209** 2014

[34] Gong X, Tong M H, Xia Y J, Cai W Z, Moon J S, Cao Y, Yu G, Shieh C L, Nilsson B and Heeger A J 2009 high-detectivity polymer photodetectors with spectral response from 300 nm to 1450 nm *Science* **325** 1665

[35] Sun H H, Jiang T, Zang Y Y, Zheng X, Gong Y, Yan Y, Xu Z J, Liu Y, Fang L, Cheng X A and He K 2017 broadband ultrafast photovoltaic detectors based on large-scale topological insulator Sb_2Te_3/STO heterostructures *Nanoscale* **9** 9325

[36] Parbatani A, Song E S, Yang F and Yu B 2018 a broadband, self-biased photodiode based on antimony telluride (Sb_2Te_3) nanocrystals/silicon heterostructures *Nanoscale* **10** 15003

[37] Yao J D, Zheng Z Q and Yang G W 2016 layered-material WS_2/topological insulator Bi_2Te_3 heterostructure photodetector

with ultrahigh responsivity in the range from 370 to 1550 nm *J. Mater. Chem. C* **4** 7831

[38] Das B, Das N S, Sarkar S, Chatterjee B K and Chattopadhyay K K 2017 topological insulator Bi_2Se_3/Si-nanowire-based p-n junction diode for high-performance near-infrared photodetector *ACS Appl. Mater. Interfaces* **9** 22788

[39] Zhang H B, Zhang X J, Liu C, Lee S T and Jie J S 2016 high-responsivity, high-detectivity, ultrafast topological insulator Bi_2Se_3/Silicon heterostructure broadband photodetectors *ACS Nano* **10** 5113